

The first term in each of these series appears also in Ref. 19. Similar results for $P_{II}(y)$ are

(i) $y \ll 1$,

$$\frac{4}{3\pi} \left(\frac{\Gamma(2/3)}{2} \right) - \frac{y^2}{4} + \left(\frac{\Gamma(10/3)}{48} \right) y^4 + \dots,$$

(ii) $y \gg 1$,

$$\frac{3}{8} \left(\frac{2}{\pi} \right)^{1/2} y^{-5/2} + \frac{3}{\pi} y^{-4} + \frac{945}{384} \left(\frac{2}{\pi} \right)^{1/2} y^{-11/2} + \dots$$

¹L. D. Bogan and D. B. Fitchen, Phys. Rev. B **1**, 4122 (1970).

²D. B. Fitchen (private communication); Reading Color Center Conference, 1971 (unpublished).

³H. Kuhnert, Phys. Status Solidi **21**, K171 (1967).

⁴L. F. Stiles, M. P. Fontana, and D. B. Fitchen, Phys. Rev. B **2**, 2077 (1970).

⁵W. H. Kleiner and W. E. Krag, Phys. Rev. Letters **25**, 1490 (1970).

⁶F. S. Ham, Phys. Rev. Letters **28**, 1048 (1972).

⁷A. M. Stoneham, Rev. Mod. Phys. **41**, 82 (1969).

⁸S. Chandrasekhar, Rev. Mod. Phys. **15**, 1 (1943).

⁹W. B. Mims and R. Gillen, Phys. Rev. **148**, 438 (1966).

¹⁰C. Chiarotti, U. M. Grassano, and R. Rosei, Phys. Rev. Letters **17**, 1043 (1966).

¹¹J. Sak, Phys. Letters **36A**, 423 (1971).

¹²R. H. Wood and U. Öpik, Phys. Rev. **179**, 783 (1969).

¹³W. B. Fowler, E. Calabrese, and D. Y. Smith, Solid State Commun. **5**, 569 (1967).

¹⁴D. M. Larsen, Phys. Rev. B **2**, 4209 (1970).

¹⁵D. Y. Smith, Solid State Commun. **8**, 1677 (1970).

¹⁶W. B. Fowler, J. Luminescence **1/2**, 755 (1970).

¹⁷H. S. Bennett, Phys. Rev. B **3**, 2763 (1971).

¹⁸R. J. Loader, thesis (Reading University, 1969), (unpublished).

¹⁹S. Chandrasekhar and J. Von Neumann, Astrophys. J. **95**, 489 (1942).

PHYSICAL REVIEW B

VOLUME 6, NUMBER 8

15 OCTOBER 1972

Identification of Optical-Absorption Bands in uv-Irradiated Potassium Azide

Larry D. Bogan and Ralph H. Bartram*

*Physics Department and Institute of Materials Science,
University of Connecticut, Storrs, Connecticut 06268*

and

Frank J. Owens

Feltman Research Laboratories, Picatinny Arsenal, Dover, New Jersey 07801

(Received 29 March 1972)

The optical-absorption bands of uv-irradiated potassium azide are correlated with the electron-spin-resonance (ESR) spectra of previously identified defects by comparison of thermal annealing kinetics. The bands which peak at 580, 700, and 780 nm are attributed to the N_4^- defect, since their annealing kinetics are identical, with an activation energy of 0.92 ± 0.09 eV. The thermal conversion of the 565-nm band to the 580-, 700-, and 780-nm bands closely resembles that of the N_2^- defect to the N_4^- defect, and, accordingly, the 565-nm band is tentatively attributed to the N_2^- defect. The activation energy for the thermal conversion of the optical spectrum is 0.70 ± 0.05 eV. No ESR spectrum could be correlated with the 360-nm band, which annealed below 140 K. All of the observed optical transitions are polarized perpendicular to the c axis. Models are proposed for the electronic structure of N_2^- , and of N_4^- in a rectangular conformation, which account qualitatively for the observed optical and ESR spectra.

I. INTRODUCTION

Color centers can be produced in the alkali azides (NaN_3 , KN_3 , RbN_3 , and CsN_3) by uv light and ionizing radiation. The phenomenon has been of interest for some time in that the defects produced are thought to be involved in the process of photochemical decomposition.^{1,2} It is therefore important that the nature of the color centers be understood in order to illuminate the mechanism of photochemical decomposition.

The object of this study is to attempt to identify

the optical-absorption bands in uv-irradiated KN_3 by means of a detailed comparison of the properties of the paramagnetic defects and optical-absorption bands that have been observed. The nature of the thermal annealing kinetics of both the electron-spin-resonance (ESR) and the optical spectra are compared and the optical bleaching properties determined. The characteristics of the growth of the spectra with dosage and intensity of the uv light are investigated. The optical-absorption spectrum is interpreted in terms of the electronic structure of the paramagnetic defects.

The structure and the properties of the azide compounds have been described in detail in a number of review articles.³⁻⁵ The azide ion is a linear N_3^- ion. The azides are unstable and can undergo thermal decomposition resulting in the evolution of nitrogen gas.⁶ They are also susceptible to photolytic decomposition. The heavy metal azides [e.g., $Pb(N_3)_2$, AgN_3] are explosively unstable whereas the alkali azides are considerably more stable.

Potassium azide has a body-centered tetragonal unit cell. The linear azide ions have two distinct orientations in the unit cell parallel to the $[110]$ and the $[1\bar{1}0]$ directions. Figure 1 shows the tetragonal structure of the unit cell of potassium azide. Both RbN_3 and CsN_3 also have this structure.

The fundamental absorption spectrum of KN_3 has been studied by Deb⁷ and Sharma and Fair.⁸ Thin films of these materials show an intrinsic absorption which has abundant structure in the region from 250 to 140 nm. An absorption band at 220 nm seems consistent with a low-lying transition of the azide ion. Although Deb has ascribed detailed structure on the shorter-wavelength bands to Wannier excitons, Sharma finds that this latter absorption is most likely due also to a low-lying transition of the azide ion and that the observed structure is of vibrational origin. Beyond 220 nm, KN_3 is normally transparent out to the far infrared where the azide ion vibrational absorptions occur.

The production of color centers in KN_3 has been studied by a number of workers.^{1,9-12} However, these investigations have not led to any definitive models for the color centers. The optical-absorption spectrum produced by uv or x-ray irradiation at liquid-nitrogen temperatures consists of a prominent visible band (VIS) at 565 nm, a much weaker

band in the near infrared (IR) at 780 nm, and a band in the near ultraviolet (uv) at 360 nm. The optical-absorption spectrum of a sample of uv-irradiated KN_3 is shown in Fig. 2. The VIS band has been assigned to the F center by previous investigators because of its qualitative similarity to the F band in KCl produced by x-ray irradiation. However, no further evidence was presented to justify this assignment, thus making the proposal only speculative. The uv band exhibits a weak structure and can be produced with much greater optical density by x irradiation than by uv irradiation. This band is the most unstable and anneals below $-100^\circ C$. During this annealing the VIS band is observed to grow slightly. Near room temperature there occurs a thermal conversion from the VIS band to the IR band and above room temperature these bands bleach.¹⁰

Far-infrared bands typical of molecular vibrational levels have been correlated to the VIS and the IR bands by a matching of the growth and the thermal-decay curves.¹⁰ The VIS band correlates with an absorption at 1637 cm^{-1} , and the IR band with one at 1666 cm^{-1} . This suggests that these optical absorptions are associated with molecular defects rather than trapped electron centers.

A number of centers have been identified by ESR in KN_3 . However, despite detailed searches, no F -center resonances have been found. A nine-line ESR spectrum resulting from the interaction of an unpaired electron with four equivalent nitrogen nuclei has been observed.^{13,14} The spectrum, obtained in KN_3 irradiated with uv light at room temperature, was assigned to the linear N_4^- molecular ion. The linear model is open to objection since it cannot account for the equal interaction of the unpaired electron with the four nuclei. Planar-rectangular or tetrahedral conformations could explain the equal interaction. More recently, satellite lines between the main lines of the nine-line N_4^- spectra have been suggested to be due to exchange coupling between the N_4^- radicals.¹⁵ When KN_3 is irradiated with uv light at liquid-nitrogen temperatures a five-line ESR spectrum is observed.^{14,16} This spectrum is attributed to an N_2^- radical. On warming the crystal to room temperature, the N_2^- anneals and the N_4^- grows. Subjecting the material to x-ray irradiation produces the N_2^- and the N_4^- plus another defect not produced by uv light, a neutral nitrogen atom.¹⁶ The spectrum of the neutral nitrogen atom is stable up to 160 K but bleaches below 196 K. Investigations of the uv production process for the N_2^- indicate that irradiation into the 220-nm band is necessary to produce it and that energy-transfer processes may be occurring prior to decomposition in the lattice.¹⁷

Mueller and Singer¹⁸ have observed thermoluminescence and exoelectron emission in KN_3 as well

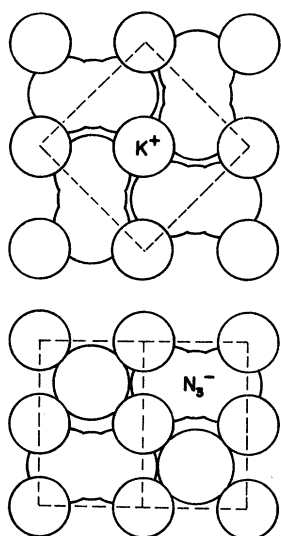


FIG. 1. Tetragonal-crystal structure of KN_3 . The upper view is along the c axis while the lower view is along the (110) direction of the crystal. The dashed lines outline the unit cell which has $c = 7.056\text{ \AA}$ and $a = 6.094\text{ \AA}$.

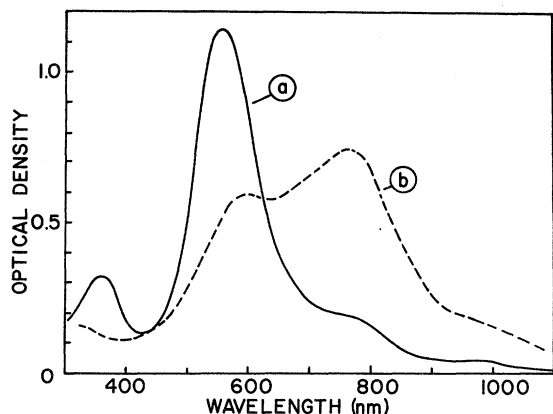


FIG. 2. Optical-absorption spectrum of KN_3 colored by uv radiation at 254 nm. Both spectra were recorded with the crystals at 77 K. Spectrum (a) results when the crystal is irradiated at 77 K while spectrum (b) occurs when the crystal is irradiated at room temperature.

as in other alkali azides. Of particular interest is a series of four glow peaks in uv-irradiated KN_3 between 80 K and room temperature. The first of these appears to correlate with the thermal bleaching of the uv band and is absent when the uv band is bleached optically. No correlation of other glow peaks with color centers is possible. Townsend¹⁹ has also investigated thermoluminescence in KN_3 induced by uv and x-ray irradiation. He found no ultraviolet-produced luminescence above 80 K but did find that the x-rayed samples showed glow peaks with similar activation energies to those found by Mueller and Singer.

The available experimental evidence is suggestive of a possible correlation between the optical bands and the ESR spectra. The fact that the N_2^- converts to the N_4^- in the same temperature range that the VIS band converts to the IR band is appealing. Also the correlation of the optical bands to the far-infrared bands lends support to the possibility that the bands are associated with molecular species. It is the object of this work to investigate in a detailed and quantitative way the possibility that the optical absorptions are associated with the paramagnetic molecular radicals that have been detected by ESR and thus provide an identification of the color centers.

II. EXPERIMENTAL PROCEDURES

All of the experiments were done on single crystals of KN_3 , most of which were grown from solution by a slow-evaporation method from starting material supplied by the Eastman Chemical Co. Some of the crystals were grown from the melt by Sharma at the Feltman Research Laboratories and were thick enough to permit polarized-absorption

measurements in any crystallographic direction. The purest solution-grown crystals are thin square platelets typically $5 \times 5 \times 0.5$ mm³ thick with the c axis normal to the platelet and the a axes at 45° to the edge. Generally these crystals were optically clear except for a small fogged spot in the center and it was usually necessary to sand and polish them in order to make the optical-absorption measurements. Thick crystals obtained from the solution in the form of a square pyramid were used for polarized-absorption studies but found to have higher concentrations of impurities as determined from additional ESR signals and absorption bands in the colored samples.

All crystals were colored with the light of the 254-nm line from a filtered high-pressure mercury arc lamp. In the case of the ESR studies, the crystals were uv irradiated in a slotted cavity fitted with a quartz system to flow cold nitrogen gas around the sample and keep it at the desired temperature. Some samples of KN_3 were colored in a liquid-nitrogen immersion Dewar while all of the samples used in the optical studies were irradiated in the optical, liquid-nitrogen cryostat.

A. Optical Experiments

A Cary model No. 14R recording spectrophotometer was used for all measurements of the optical absorption from 190 to 2500 nm. The crystals were mounted in the cryostat such that only a small clear portion of the sample was selected by the use of a mask with a 2-mm square hole. Optical-absorption measurements with various polarizations were made by placing the appropriate sheet polarizers in both the reference and sample beams of the Cary.

The thermal kinetic studies were done by the method of pulse annealing. The samples were colored and their optical density measured at 77 K at all times. Annealing of the VIS bands occurred below 0°C and was accomplished by pouring an organic liquid at its melting point into the cryostat reservoir immediately after emptying it of liquid nitrogen. In this manner the sample could be warmed from -196 to -10°C in about 1 min. Cooling down to liquid-nitrogen temperatures required about the same time. For annealing times of 5 min or more, these times were short enough to cause negligible error in the actual time at the elevated temperature. A slightly different procedure was used to anneal the IR bands in the region of 20 to 50°C . In this case compressed air was forced through the cryostat reservoir before flowing hot water of the desired temperature through it, and the warm-up time was about 3 min. Pressurized air was also used in cooling down in order to empty the reservoir of any water. All temperatures were continuously monitored with a platinum

resistance thermometer and an ac Wheatstone bridge.

B. Electron-Spin-Resonance Experiments

A Varian model No. E-3 x-band EPR spectrometer equipped with a slotted TE₂₀₁ cavity and a model No. E-4540 temperature controller was used for electron-spin-resonance measurements. All determinations of the ESR spectrum of colored KN₃ were made at -180 °C. The temperature changes required for the pulsed annealing of the N₂⁻ signal at temperatures just below 0 °C were produced with the temperature controller but those for the annealing of the N₄⁻ required that the crystal be annealed outside the cavity. This method utilized a hot oil bath at the appropriate temperature and required accurate repositioning of the sample in the cavity after annealing. Warm-up and cool-down times were fast since the samples were small and the transfer from one temperature to the other was very fast.

Optical bleaching of the ESR signals was performed in the cavity by focusing the light on the sample through the slotted wall.

III. RESULTS

A. Optical Properties

The optical-absorption spectrum produced by uv irradiation of a fresh crystal of KN₃ is shown in Fig. 2. In this case the light is propagating along the *c* axis and is unpolarized. In a pure crystal two prominent bands appear, one at 360 nm and the other at 565 nm. The weak absorption on the low-energy side of the 565-nm band grows at a different rate than the 565-nm band and its optical density depends on the purity of the crystal (see Fig. 3).

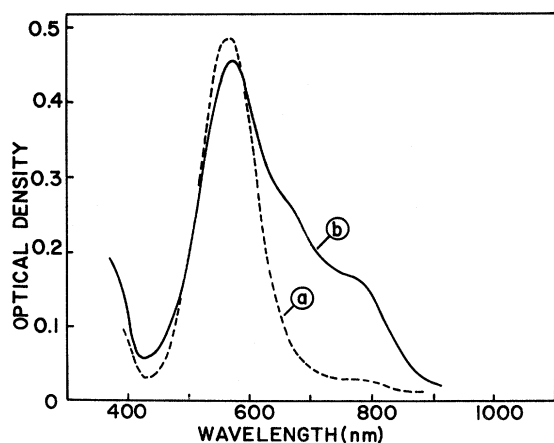


FIG. 3. Optical-absorption spectra produced by uv radiation (a) in a relatively pure crystal of KN₃ and (b) in a relatively impure crystal of KN₃. Both crystals were irradiated at 77 K.

The band at 360 nm saturates very early in the coloring process at an optical density of about 0.20 while the other bands continue to grow. The positions of these bands agree with those determined by Papazian,¹⁰ Heal and Pringle,¹¹ and Cunningham and Tompkins.⁹ However, we find that the width of the 565-nm band is only 0.42 eV as compared to 0.65 eV as determined by Papazian.

Figure 4 shows the optical absorption of a melt-grown crystal colored in the same manner as above but in this case the light is propagating perpendicular to the *c* axis along the (110) direction and is polarized either along [curve (a)] or normal [curve (b)] to the *c* axis. (Unfortunately, the bands at 700 and 780 nm are relatively large in this case indicating a comparatively large concentration of the impurities producing these bands. The same problem occurs when thick solution-grown crystals were used in the same measurements.) The important result shown here is that the only absorption occurs for light polarized in the direction perpendicular to the *c* axis.

No other radiation-induced bands were found in the optical region out to about 2.5 μm. Narrow lines in the near infrared at 1.36, 1.6, and 2.2 μm were observed and were dichroic but did not grow upon coloration. These lines are probably due to trace impurities but no identification of them was attempted.

An additional experiment was performed to determine whether the color centers responsible for the 565-nm band could be induced to have preferential absorption for either of the two directions of light polarized perpendicular to the *c* axis. Experiments²⁰ have shown that color centers can be oriented with polarized light and that the orientation will appear as a change in the polarized absorption of the absorption band. First of all, no dichroism between the [110] and [1 $\bar{1}$ 0] directions of polarization was observed in either of the bands when the KN₃ was colored with 254-nm light polarized in one of these directions. The second type of experiment attempted to produce polarized absorption by bleaching the bands at 77 K with polarized light. The 565-nm band did not bleach at all while the 360-nm band bleached rapidly but showed no dichroism in the process. The 565-nm band would not bleach even when the temperature was raised to 190 K. Light of wavelength 366, 546, and 579 nm was used to try to bleach the 565-nm band, and 366-nm light was used to bleach the 360-nm band.

Under certain conditions the optical density of the 565-nm band would change when a freshly colored crystal was irradiated with the 366-nm line of the mercury lamp. The band would grow slightly as the 360-nm band bleached if it were only two or three times the density of the 360-nm band. Continued illumination after the 360-nm band was gone

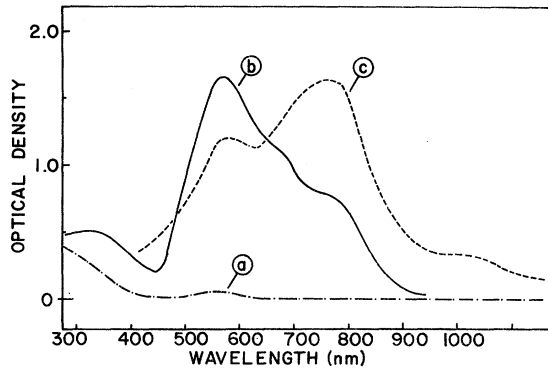


FIG. 4. Polarized absorption spectrum of KN_3 uv irradiated and measured at 77 K. Light propagates along the (110) direction. Curve (a) is the absorption for light polarized parallel to the c axis of the crystal; curve (b) is the absorption for light polarized perpendicular to the c axis; and curve (c) is the absorption for light polarized perpendicular to the c axis after the crystal has been warmed to room temperature for 15 min and recooled. The absorption of light polarized parallel to the c axis after warmup was unchanged from that given by curve (a).

would then partially bleach the 565-nm band especially if there were impurity bands present.

The optical absorption produced by coloring at room temperature is shown in Figs. 2 and 5. There is no 360-nm band and the absorption extends from 450 through 1100 nm. The best fit to this band of absorption requires at least four Gaussian bands and the four used here are shown in Fig. 5. The very broad Gaussian shown with a peak at 830 nm is present or not present depending on the thermal treatment of the crystal after coloration. The data used in Fig. 8 were selected to show the presence of the 830-nm band. All the bands involved are only metastable at room temperature and decay to about half their height in 16 h. They are, however, stable against optical bleaching at both 77 K and room temperature.

B. Thermal Properties of Optical Bands

The 360-nm band anneals first as the colored crystal is warmed from 77 K. Figure 6 shows the irreversible decrease in the band height at a warm-up rate of 2 K per min and the maximum rate of anneal occurs at about 137 K. This curve can be fitted by assuming that first-order kinetics govern the annealing process and as a result the rate of change of the number of centers N is given by

$$\frac{dN}{dt} = sN e^{-\Delta E/kT},$$

where s is the frequency factor and ΔE is the activation energy for the process. A plot of $(dN/dT)/N$ vs $1/T$ for the constant warm-up rate dT/dt yields $\Delta E = 0.20 \pm 0.02$ eV and $s = 10^3$ to 10^4 sec $^{-1}$. The

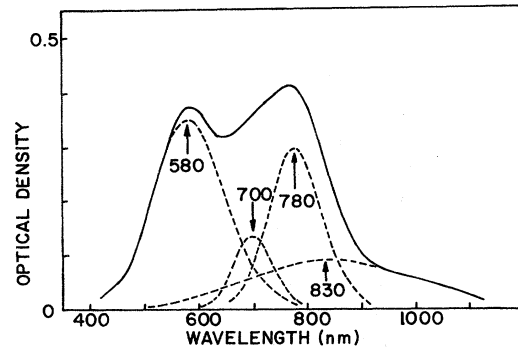


FIG. 5. Resolution of the absorption bands into Gaussian band components. The spectrum is that of color centers produced by uv irradiation at room temperature, measured at 77 K. The heights and widths of the individual bands were selected to give the best fit with the least number of bands.

extremely low frequency factor s suggests that the assumption of first-order kinetics is not justified. The data were fitted nearly as well by the assumption of second-order kinetics,

$$\frac{dN}{dt} = (N^2/N_0) s e^{-\Delta E/kT},$$

with parameters $\Delta E = 0.45 \pm 0.05$ eV and $s = 10^{13} - 10^{16}$ sec $^{-1}$, where N_0 is taken to be the initial concentration. It was not feasible to perform pulsed annealing experiments for this band to determine the kinetics with certainty. Figure 6 also shows some structure on the low-energy side of the band which has an estimated separation of 1200 cm^{-1} corresponding to a typical vibrational frequency. This structure disappears during the annealing process.

In contrast, the optical absorption in the region of the 565-nm band is not reduced to zero during the annealing of this band. As the crystal is warmed, infrared bands at about 700 and 780 nm appear and the 565-nm band disappears but another band at 580 nm grows in its place. This behavior

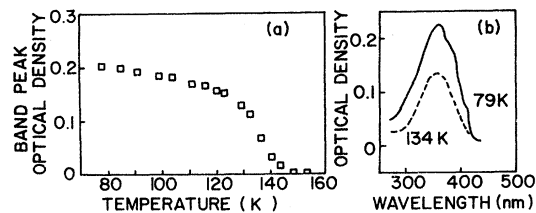


FIG. 6. (a) Height of the peak of the 360-nm band as a function of temperature. The warm-up rate was a constant 2.0 K per min. (b) Absorption shape of the 360-nm band at 79 and 134 K measured during the warm-up procedure.

is shown in Fig. 7; note that the band which occurred at 800 nm when the crystal was initially colored anneals by 250 K, and is not the same absorption that grows at higher temperatures. The warm-up rate will determine the shape of the optical absorption at each temperature and these data were obtained with a warm-up rate that varied from 2 to 1 K per min. An analysis like that used on the 360-nm band is not possible because the bands become very broad and overlap too much to be analyzed separately.

By using the technique of pulsed annealing with the optical absorption recorded at 77 K, the growing and decaying bands can be separated. Figure 8 shows the results of pulsed annealing at -23°C and Fig. 9 shows the relative heights of the optical absorption vs time at 565 nm obtained at four different annealing temperatures. The band at 580 nm grows and anneals at the same rate as those at 700 and 780 nm and maintains an area of 72% of these bands. This fact allowed the use of the measured areas of the 700- and 780-nm bands to determine the amount of the 580-nm band to be subtracted from the 565-nm band to give the true area of the 565-nm band. The result of this analysis gives the true decay of this latter band which is shown in Fig. 10. The decay is exponential in time which indicates that the kinetics involved are first order. The activation energy obtained from a plot of the logarithm of the decay times vs inverse temperature (Fig. 11) is 0.70 ± 0.10 eV. The frequency term is approximately $3 \times 10^{10} \text{ sec}^{-1}$.

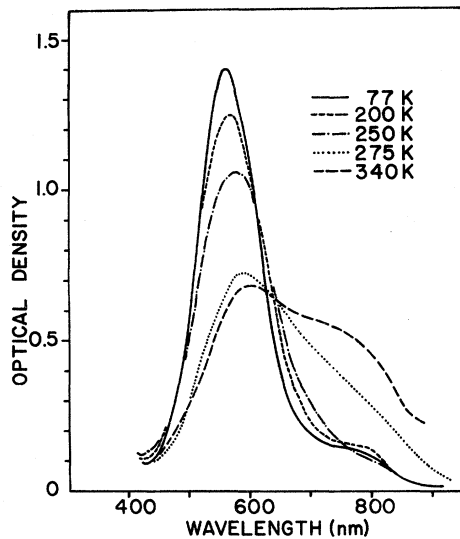


FIG. 7. Absorption spectrum of the 565-nm band at various temperatures during a slow warmup of the crystal from 77 K to room temperature. The rate was 2 K per min at 77 K but decreased to about 1 K per min near room temperature.

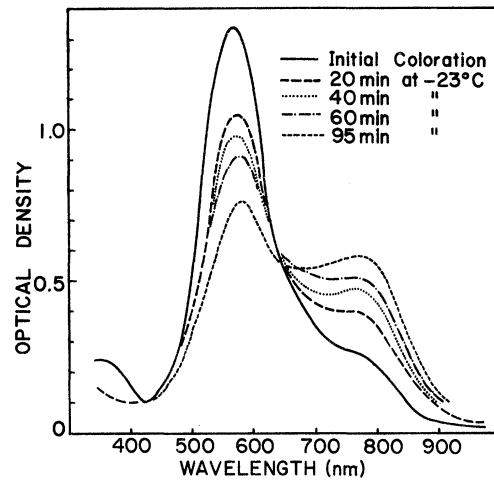


FIG. 8. Absorption spectrum of the 565-nm band measured at 77 K as affected by increasing total time spent at 250 K (pulsed annealing). After the initial period at 250 K the area under the absorption bands is constant.

The thermal properties of the 580-, 700-, and 780-nm bands were studied in the region of 20 to 60°C by the same type of pulsed annealing. In this case there were no underlying bands to complicate the analysis. The only difficulty occurs with the treatment of the 830-nm band when it must be subtracted from the absorption. In the range from 20 to 30°C this band did not anneal relative to the other bands while from 50 to 60°C it seems to anneal as rapidly.

The data for the heights of the 580- and 780-nm bands as a function of time for several annealing temperatures are shown in Fig. 12. The data

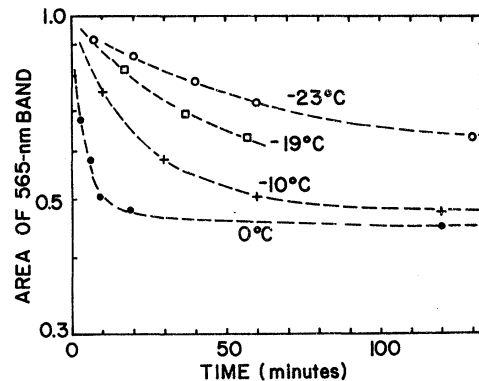


FIG. 9. Area of the absorption band at 565 nm as a function of pulsed annealing times at four different temperatures. The areas are relative to that of the absorption band before annealing. All absorption spectra were recorded at 77 K. Here the area of the 565-nm band is defined as that of a Gaussian component which has the shape of the band before annealing.

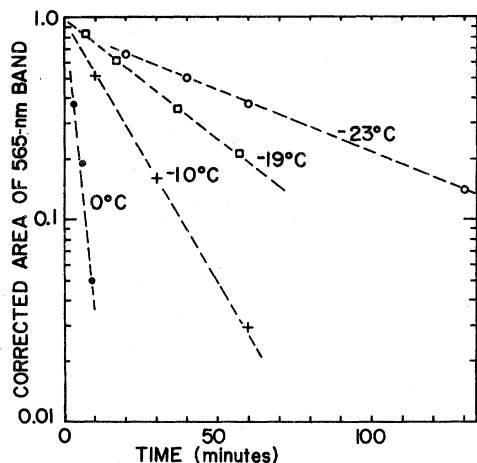


FIG. 10. Area of the 565-nm band as a function of time of annealing at four different temperatures. This is derived from the same data as Fig. 9 but the area of the 565-nm band is now determined after a band at 580 nm is subtracted from the spectrum. The fact that the 580-nm band grows and anneals at the same rate as the 780-nm band was used to determine the area of the 580-nm band. The slopes of the lines fit to the data give the average annealing times.

show the semilogarithmic dependence typical of first-order kinetics. The decay times then determine the activation energy to be 0.92 ± 0.10 eV and the characteristic frequency to be about 10^{11} sec $^{-1}$,

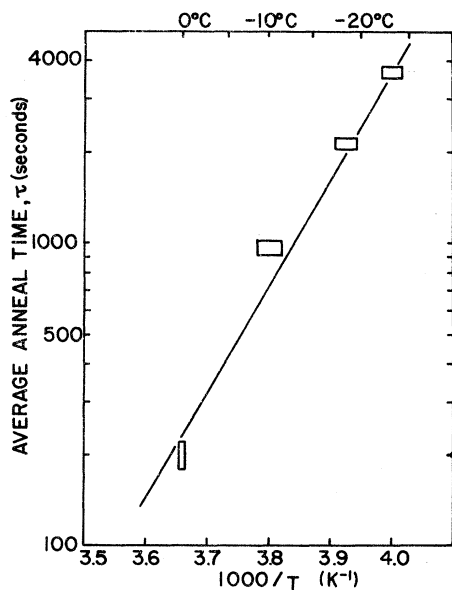


FIG. 11. A plot of the average annealing times at the four temperatures 0, -10, -19, and -23°C as a function of $1000/T$. The slope of the lines yields an activation energy of 0.70 eV and the intercept gives $s = 3 \times 10^{10}$. The size of the boxes reflects the probable errors in τ and T .

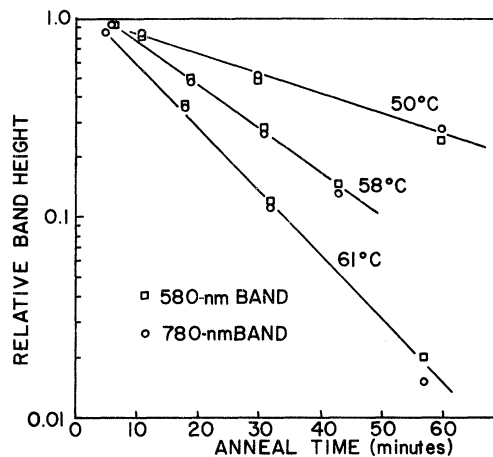


FIG. 12. Relative optical density at 580 and 780 nm as a function of time at three annealing temperatures. The relative optical density is taken with respect to the unannealed spectrum such as given by curve (b) in Fig. 2. All the data come from absorption spectra of the color centers produced by uv irradiation at room temperature, as measured at 77 K (pulsed annealing).

as shown in Fig. 13.

C. Electron Spin Resonance

When potassium azide is uv irradiated at 77 K, the predominant ESR signal is that due to the N_2^- . Other signals are also present, some of which are the lines due to impurities of oxides of nitrogen as reported by Mergerian and Marshall.²¹ The nine-line hyperfine spectrum of the N_4^- is produced when the crystal is warmed to room temperature or colored at room temperature. The properties of the N_4^- ESR signal were as reported by previous investigators.^{13,14} We saw some other small signals not previously reported, but made no attempts to identify them. None appeared to have the same thermal properties as the 360-nm band.

Several runs were made to determine the thermal characteristics of the conversion of the N_2^- ESR signal into the N_4^- signal. A new crystal was used at each temperature in the pulsed annealing procedure since the end products of an anneal might affect following experiments on the same crystal. Unfortunately, the results are not consistent. Two runs for each of four annealing temperatures are shown in Fig. 14. The annealing rates change such that it is impossible to extract characteristic decay times and hence no activation energy could be estimated. Some of the problems that occur in these experiments are the difficulty of coloring each sample to the same extent and the inaccuracies of subtracting background ESR lines that underlie the N_2^- spectrum.

The growth rate of the N_2^- signal seems to be

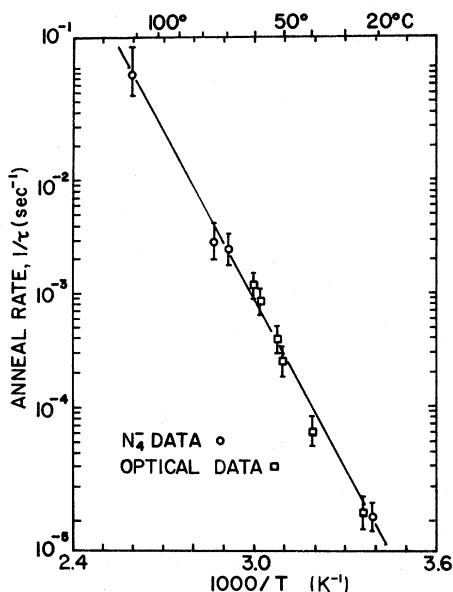


FIG. 13. Average anneal rate $1/\tau$ vs the inverse of the temperature of annealing. The circles are determined from the annealing of the N_4^- ESR signal at 77 K. The squares are determined from the annealing of the optical absorption of the room-temperature color centers at 580 and 780 nm as given in Fig. 13. Both sets of data are fitted by the line which represents an activation energy of 0.92 eV with $s = 8 \times 10^{10} \text{ sec}^{-1}$.

proportional to the square of the uv light intensity, and shows an interesting dependence on the polarization of the uv light.¹⁷

The pulse annealing of the N_4^- at temperatures up to 70 °C produced reliable data and the anneal times vs inverse temperature are plotted with the same data for the IR bands in Fig. 13. The N_4^-

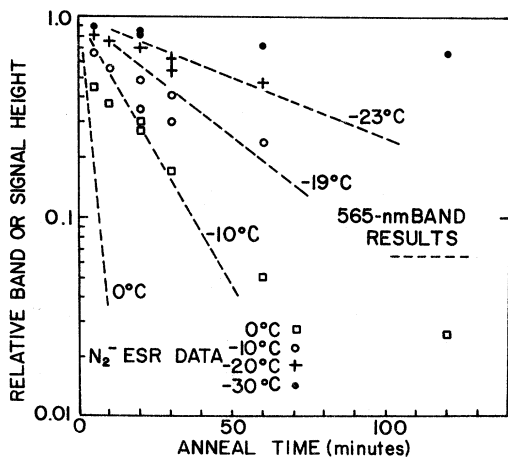


FIG. 14. Pulsed annealing data of the N_2^- ESR signal at 77 K are compared with the corresponding data of Fig. 10 for the 565-nm band.

growth is linear in the intensity of the uv light and the time of irradiation. This is shown by the data given in Fig. 15.

IV. DISCUSSION

It can be seen from Fig. 13 that the pulsed annealing of both the room-temperature optical-absorption bands at 580, 700, and 780 nm and the N_4^- ESR spectrum follows first-order kinetics with an activation energy of 0.92 eV and an attempt frequency of $8 \times 10^{10} \text{ sec}^{-1}$. On the basis of the excellent correlation of these data, the 580-, 700-, and 780-nm bands are ascribed to the N_4^- defect. The association of these bands with a molecular defect is supported by Papazian's¹⁰ correlation of the same optical-absorption spectrum with a far-infrared band at 1666 cm^{-1} .

The thermal conversion of the low-temperature optical-absorption band at 565 nm to the room-temperature bands at 580, 700, and 780 nm was compared with the thermal conversion of N_2^- to N_4^- as determined by ESR, but with less conclusive results. The thermal conversion of the optical bands followed first-order kinetics, with an activation energy of 0.70 eV and an attempt frequency of $3 \times 10^{10} \text{ sec}^{-1}$. The thermal conversion of the ESR spectrum for N_2^- to that for N_4^- occurs in the same temperature range, but does not seem to fit

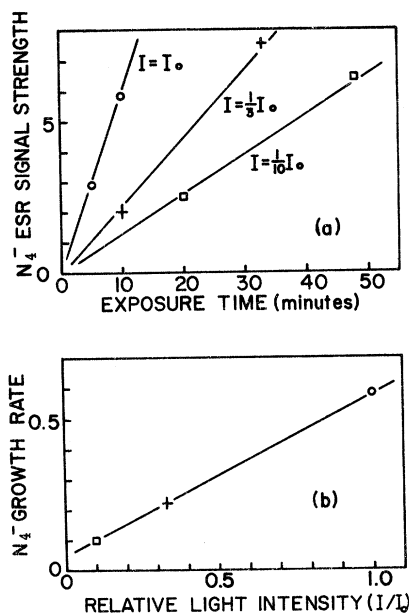


FIG. 15. (a) Signal strength of the N_4^- ESR signal as measured at 77 K as a function of the time of irradiation with ultraviolet light at 254 nm with the crystal at room temperature. Three different intensities were used. (b) A plot of the N_4^- growth rate as determined from the slopes of the (a) part of this figure vs relative light intensity used.

any order of kinetics. It is noteworthy that the initial slopes on a semilog plot of the ESR conversion curves in Fig. 14 match those of the optical conversion curves, but the ESR curves tend to level off with time. It seems probable that the same process is involved in both the optical and ESR conversions, but that the discrepancy arises from the very much higher concentration of centers required for the ESR experiment. For example, in the ESR case, the rate of thermal conversion may decline because of the high concentration of the end products (N_4^- ions and vacancies).

On the basis of this tentative correlation of the thermal conversion of optical-absorption spectra with ESR spectra, and the previous identification of the 580-, 700-, and 780-nm bands with N_4^- , we ascribe the 565-nm band to the N_2^- defect. Papazian's¹⁰ correlation of the 565-nm band with a far-infrared band at 1637 cm^{-1} supports a molecular model. The infrared activity of the N_2^- may result from a perturbation which removes the inversion symmetry.

The annealing of the 360-nm band at very low temperature was not correlated with any other process, and thus there is no present basis for further speculation about the identity of the corresponding defect.

It is of interest to identify the electronic transitions of the molecule ions which are responsible for the observed optical spectra. Apart from the transition energies, the principal qualitative feature to be explained is the dichroism; all observed transitions are polarized perpendicular to the crystal c axis. (Absorption line shapes, which involve interaction of the electronic system with both

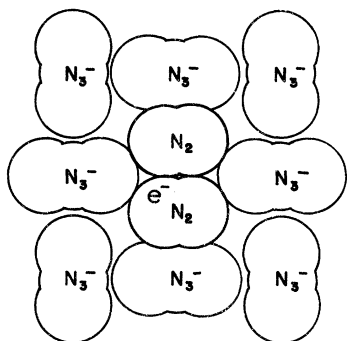


FIG. 16. Rectangular model for the N_4^- defect. A cross section of a KN_3 crystal perpendicular to the c axis and in the plane of the azide sites is shown. Here one azide ion is replaced with two nitrogen molecules (N_2) whose sizes are determined by their covalent radii and interatomic spacing. The extra electron is assumed to be delocalized in a bonding orbital. The size of the azide ion is that determined from an ionic size required to fit in the alkali azides with the tetragonal structure.

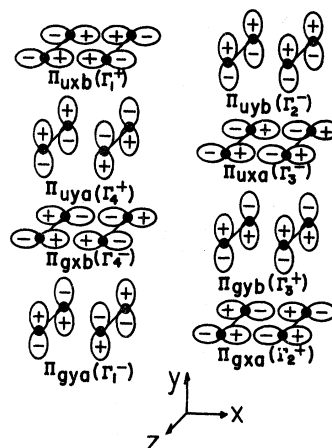


FIG. 17. Schematic representation of molecular orbitals of the rectangular N_4^- , made of linear combinations of the π_u and π_g orbitals of the N_2 molecule. The orbitals are labeled in an obvious notation, and also by the irreducible representations of D_{2h} .

molecular and lattice vibrations, will not be considered here.)

The N_2^- molecule ion is isoelectronic with the well-known molecule ion O_2^+ .²²⁻²⁴ The ground configuration is $(1\sigma_g)^2 (1\sigma_u)^2 (2\sigma_g)^2 (2\sigma_u)^2 (3\sigma_g)^2 (1\pi_u)^4 (1\pi_g)$. (The order of $3\sigma_g$ and $1\pi_u$ is uncertain, but immaterial.) We ascribe the 565-nm band to the lowest transition of the form: $\dots (1\pi_u)^4 (1\pi_g)$, ${}^2\Pi_g \rightarrow \dots (1\pi_u)^3 (1\pi_g)^2, {}^2\Pi_u$. This transition is observed in O_2^+ only in emission. The zero-phonon line occurs at 4.7 eV, and the peak of the absorption band would occur at 5.5 eV.^{22,24} One expects a substantial reduction in the transition energy in going from O_2^+ to N_2^- , so it is not unreasonable to postulate that the corresponding absorption band peaks at 2.2 eV in N_2^- . This transition is polarized parallel to the molecule axis, and consequently perpendicular to the crystal c axis, as required. (The N_2^- ions are assumed to occupy anion sites and are aligned parallel to the missing azide ion.¹⁶)

In order to explain the room-temperature optical-absorption spectrum, one must postulate a geometry for the N_4^- defect. This defect was identified by its ESR spectrum, and was originally described as linear.¹³ However, a linear conformation is not compatible with the observed hyperfine splitting, which is interpreted in terms of equal hyperfine interactions with all four nuclei. An alternative conformation which is compatible both with the hyperfine splitting and the site symmetry is a rectangular N_4^- occupying a single anion site, as shown in Fig. 16. This molecule ion may be thought of as a pair of N_2 molecules which share an extra electron in a bonding orbital. The N_2 molecule is about 3.0 Å in diameter and 4.1 Å

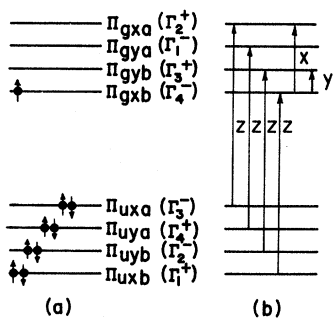


FIG. 18. (a) Probable order of the one-electron energies associated with the N_4^- molecular orbitals shown in Fig. 17. The occupancy is indicated for the ground configuration. (b) Allowed electric dipole transitions are shown with their polarizations. Directions x , y , and z refer to the coordinate axes in Fig. 17. y is along the c axis of the crystal.

long²⁵; two such molecules would fit tightly in one azide site.

Molecular orbitals of N_4^- made up of symmetry-adapted combinations of π_u and π_g orbitals of N_2 are shown schematically in Fig. 17. These orbitals are labeled in an obvious notation, and also by the irreducible representations of D_{2h} . The probable order of the corresponding one-electron energies is shown in Fig. 18, and the population of the orbitals in the ground configuration is indicated. Also shown in Fig. 18 are the allowed transitions. The symmetry of the ground state is determined by the single unpaired electron to be ${}^2\Gamma_4^-$. The four transitions labeled z are polarized parallel to the z axis (perpendicular to the crystal c axis) and are all to ${}^2\Gamma_1^+$ states, whose interaction removes the apparent degeneracy. Note that these symmetry designations refer to the many-electron states, and should not be confused with the labeling of one-electron orbitals.

We ascribe the 580-nm band to the lowest-energy transition of this type, ${}^2\Gamma_4^- \rightarrow {}^2\Gamma_1^+$, which is analogous to the lowest ${}^2\Pi_g \rightarrow {}^2\Pi_u$ transition of N_2^- . The transition labeled x (${}^2\Gamma_4^- \rightarrow {}^2\Gamma_2^+$) is also polarized perpendicular to the c axis, and must then correspond to the 780-nm band. Note that this transition is internal to the states arising from π_g orbitals of N_2 , and appears as a consequence of formation of the N_4^- molecule ion. Only the y transition (${}^2\Gamma_4^- \rightarrow {}^2\Gamma_3^+$) is polarized parallel to the c axis; however, it may well occur at a wavelength beyond the $2\text{-}\mu$ limit of the instrument, and in any event it is apparent from the orbitals in Fig. 17 that the corresponding oscillator strength should be relatively small.

The unpaired spin occupies the $\pi_{gxb}(\Gamma_4^-)$ orbital, which clearly has equal hyperfine interactions with the four nuclei. Furthermore, it is evident that the y and z components of the hyperfine tensor \bar{A} should be nearly equal while the x component should be substantially different; i. e., the unique component should be perpendicular to the c axis and parallel to the axis of the missing azide ion, which is in fact what has been observed.¹³ (The orbitals depicted in Fig. 17 are oversimplified; actually, the contact and anisotropic hyperfine interactions are comparable.)

In summary, it is apparent that the N_2^- model can explain the optical-absorption spectrum at 77 K, including the observed dichroism. Similarly the rectangular N_4^- model can explain the optical spectrum at room temperature and is consistent with the observed hyperfine splitting of the ESR spectrum.

ACKNOWLEDGMENT

We are grateful to Dr. J. Sharma of the Feltman Research Laboratories at Picatinny Arsenal for supplying samples of melt-grown KN_3 .

*Supported in part by the U. S. Army Research Office—Durham under Contract No. DA-ARO-D-31-124-71-G35.

¹P. W. M. Jacobs and F. C. Tompkins, Proc. Roy. Soc. (London) **A215**, 254 (1952).

²J. C. Dodd, J. Chem. Phys. **35**, 1815 (1961).

³B. L. Evans, A. D. Yoffe, and P. Gray, Chem. Rev. **59**, 515 (1959).

⁴P. Gray, Quart. Rev. (London) **17**, 441 (1963).

⁵A. D. Yoffe, in *Inorganic Nitrogen Chemistry*, edited by C. B. Colburn (Elsevier, New York, 1966), Vol. 1, p. 73.

⁶P. W. M. Jacobs and F. C. Tompkins, Proc. Roy. Soc. (London) **A215**, 265 (1952).

⁷S. K. Deb, J. Chem. Phys. **35**, 2122 (1961).

⁸J. Sharma and H. D. Fair, Bull. Am. Phys. Soc. **15**, 387 (1970).

⁹J. Cunningham, and F. C. Tompkins, Proc. Roy. Soc. (London) **A251**, 27 (1959).

¹⁰H. A. Papazian, J. Phys. Chem. Solids **21**, 81 (1961).

¹¹H. G. Heal and J. P. S. Pringle, J. Phys. Chem. Solids **15**, 261 (1960).

¹²F. C. Tompkins and D. A. Young, Proc. Roy. Soc. (London) **A236**, 10 (1956).

¹³A. J. Shuskus, C. G. Young, O. R. Gilliam, and P. W. Levy, J. Chem. Phys. **33**, 622 (1960).

¹⁴H. B. Horst, J. H. Anderson, and D. E. Milligan, J. Phys. Chem. Solids **23**, 157 (1962).

¹⁵F. J. Owens, Phys. Letters **33A**, 41 (1970).

¹⁶D. W. Wylie, A. J. Shuskus, C. G. Young, O. R. Gilliam, and P. W. Levy, J. Chem. Phys. **33**, 622 (1960).

¹⁷F. J. Owens, Phys. Rev. B **2**, 2064 (1970).

¹⁸H. Mueller and G. D. Singer, Z. Physik **182**, 366 (1965).

¹⁹P. Townsend, J. Chem. Phys. **2**, 1116 (1969).

²⁰See, for example, the review article by W. B. Fowler, in *Physics of Color Centers*, edited by W. B. Fowler (Academic, New York, 1968).

²¹D. Mergerian and S. A. Marshall, Phys. Rev. **127**,

2015 (1962).

²²V. M. Ellsworth and J. J. Hopfield, *Phys. Rev.* **29**, 79 (1927).²³R. S. Mulliken, and D. S. Stevens, *Phys. Rev.* **44**,

720 (1933).

²⁴R. W. Nicholls, *Can. J. Phys.* **43**, 1390 (1965).²⁵R. C. Evans, *Crystal Chemistry* (Cambridge U. P., Cambridge, England, 1966), pp. 74 and 112.

PHYSICAL REVIEW B

VOLUME 6, NUMBER 8

15 OCTOBER 1972

Oblique Polaritons in Uniaxial Crystals: Application to LiIO_3 [†]

W. S. Otaguro, E. Wiener-Avneer,* S. P. S. Porto, and J. Smit

Departments of Physics and Electrical Engineering, University of Southern California, Los Angeles, California 90007

(Received 28 January 1972)

In Raman scattering involving polaritons propagating at arbitrary oblique angles with respect to the crystallographic axes, the selection rules derived for polaritons propagating along the crystal axes are no longer obeyed. We present the analysis of oblique polaritons which account for their frequency dispersion as a function of both the magnitude and the direction of the wave vector \vec{k} . Application of this theory to the experimental results obtained for LiIO_3 easily clarifies the appearance of "new" lines in the polariton region.

INTRODUCTION

Raman scattering for phonons propagating along the crystallographic axes is well understood in terms of the selection rules provided by group theory.¹ Also, the dispersion in the polariton region associated with the variation of the magnitude of the wave vector \vec{k} of the phonon, again directed along the crystallographic axes, has been shown to agree with theory.²⁻⁵ However, when the phonon is not propagating along the crystallographic axis (oblique phonon), "new" frequencies occur which seem to violate the selection rules.

The occurrence of this angular dispersion was first noted by Poulet,⁶ by Ketelaar *et al.*,⁷ and by Couture-Mathieu *et al.*⁸ An approximate theory for the angular dispersion in crystals with two atoms per unit cell was given by Loudon.⁹ This theory was used for the Raman effect by Damen *et al.*¹⁰ in the study of the Raman spectra of ZnO. Arguello *et al.*¹¹ provided an extensive discussion of Loudon's model in their analysis of the first-order Raman effect in wurtzite-type crystals. These early works merely analyzed the Raman spectra where the phonons outside of the polariton region were propagating midway between two crystallographic axes. An attempt was made to study the experimental results of angular dispersion in LiIO_3 for 90° Raman scattering.¹² Although the agreement between the theory and the experimental results was fair, LiIO_3 , being a uniaxial crystal with C_6^2 symmetry and two molecules per unit cell, presented a more complicated problem than that of the wurzite crystals upon which Loudon's derivations were based.⁹ It was evident that a more general expression for the angular

dispersion was needed.

In studying NaNO_2 Hartwig *et al.*¹³ used the electrostatic approximation to explain the angular dispersion of the oblique phonons outside the polariton region ($k^2 c^2 / \omega^2 > \epsilon_0$). For oblique phonons propagating in a major crystallographic plane, frequency gaps occur. The frequency gaps are determined by the transverse optic (TO) and longitudinal optic (LO) end-point frequencies, which characterize the phonons propagating along the crystallographic axes with monotonically varying angular dispersion curves. Using Eq. (3) of Ref. 13 for the angular dispersion in LiIO_3 studied earlier,¹² the agreement between experiment and theory was excellent.¹⁴ Thus the angular dispersion outside the polariton region is quite well explained. However, in the polariton region, the electrostatic approximation is no longer valid.¹³ The derivation of the angular dispersion must now include the magnetic fields.

We report the theoretical and experimental re-

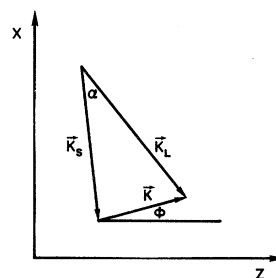


FIG. 1. Conservation of momentum. The forward-scattering angle is represented by α . The angle between the propagation direction of the polariton and the z axis is represented by ϕ .